Extended kinetic theory applied to inclined granular flows: role of boundaries.

Devis Gollin · Diego Berzi · Elisabeth T. Bowman

Abstract We compare the predictions of Extended Kinetic Theory (EKT), where the roles of surface friction and correlation in fluctuation velocities are taken into account, with discrete element simulations of steady, fully-developed, inclined flows of identical spheres over bumpy bases, in the presence and absence of flat, frictional sidewalls. We show that the constitutive relation for the pressure of EKT must be modified in the proximity of the boundary, because of the influence of excluded volume and shielding associated with collisions of particles with the boundary itself. We also note that currently available boundary conditions for flows over bumpy planes in kinetic theory underestimate the energy dissipation. These two observations explain the lack of agreement of EKT with the simulations, in terms of the maximum angles of inclination for which steady, fully-developed flows are possible. That is, for some high angles of inclination, EKT does not have solutions, while steady flows are predicted in DEM. However, whenever a solution to the system of differential equations of EKT does exist, the predicted distributions of velocity, solid volume fraction and granular temperature satisfactorily match the numerical measurements. The incompressible, algebraic approximation of EKT, which ignores the conduction of energy in the energy balance, admits solutions for a wider range of angles of inclination, as in the simulations, but fails to reproduce the quantitative and qualitative behaviour of solid volume fraction and granular temperature in the two conductive layers at the top and bottom of the flow. When frictional sidewalls are added to the domain, we show that the spanwise ratio of shear stress to pressure is linearly distributed in the dense core region of the flow, confirming that the sidewalls exert, on average, a Coulomb-like resistance to the flow with an effective friction coefficient which is less than half the actual particle-wall friction.

Keywords Kinetic theory · Discrete Element Method · Inclined flow · Bumpy base

D. Gollin
Department of Civil and Structural Engineering, University of Sheffield, Sheffield, S10 2TN, UK. E-mail: devis.gollin@sheffield.ac.uk

D. Berzi
Department of Civil and Environmental Engineering, Politecnico di Milano, Milano, 20133, Italy. E-mail: diego.berzi@polimi.it

E.T. Bowman
Department of Civil and Structural Engineering, University of Sheffield, Sheffield, S10 2TN, UK. E-mail: e.bowman@sheffield.ac.uk

1 Introduction

Flowing granular materials driven by gravity are encountered in a diverse range of geophysical contexts such as rock avalanches, landslides and debris flows and in a variety of industrial processes involving handling and transporting of bulk materials. Considerable research has been undertaken in the last few decades to develop a fundamental understanding of this class of materials. Although significant progress has been made, complete constitutive models that are able to fully characterize the behaviour of these flows still remains a challenge for engineers and physicists alike.

At present, even the simple case of steady, fully-developed, dry granular flows comprised of identical, nearly spherical, rigid particles is not completely understood. Furthermore, even though isolated physical mechanisms are well described, their inclusion in one general model is still problematic.

Inclined chute geometries have been widely used to investigate the mechanics of granular flows. Experimental [1–4] and numerical [5–8] works usually find common agreement and help their constitutive description. However, simply changing the boundary conditions (bottoms and sidewalls), slope angles and flow rates produces remarkably different behaviours. Over a flat base, a shallow flow behaves as an agitated and dilute layer while, for increasing flow depth, a large region of plug flow with high slip velocity and vanishing shear rate develops [9]. Conversely, a rough bottom generally reduces slip at the base while sustaining a sheared flow. In this case, depth-averaged velocities strongly depend on inclination and flow height, which, in turn, determine whether a flow stops, steadily propagates or constantly accelerates [2, 6]. It is also seen that sidewalls have the dual effect of supporting flows over rough bases at increasingly high slope angles and stabilizing flowing piles over erodible surfaces of heaps at inclinations greater than the angle of repose [10, 4, 9].

When the flowing system is dilute, it is commonly accepted that particles mainly interact through instantaneous, binary, uncorrelated collisions. Assuming that this process is the main mechanism of energy dissipation, classic kinetic theory of granular gases [11–13] has been found to describe the regime. However, in any practical application, gravity typically acts to collapse the flows into denser system, where the solid volume fraction, ν, can exceed the freezing point at which a phase transition to a crystalline state is first possible (0.49 for monosized spheres [14]). In this dense regime, it is widely considered that kinetic theory is not a good candidate for describing granular flows, because of the role of frictional, long-lasting contacts and the fact that collisions are no longer perceived as binary, instantaneous and uncorrelated. As a consequence, a very popular approach has been proposed based on a phenomenological local rheology that links the stress ratio (ratio of shear stress to pressure) to the inertial parameter (shear rate made dimensionless using the pressure, particle density and diameter) [15]. It suits flow regions well, where the density is uniform; however, it fails close to the boundaries [16], and in describing phase transitions [17].

A more fundamental approach that relies on extensions of classic kinetic theory has emerged as a valid alternative. The role of particle friction has been included in the collisional dissipation rate of translational, fluctuation energy through an effective coefficient of restitution [18, 19]. The breaking of the molecular chaos assumption at solid volume fractions larger than 0.49 has been shown to mainly decrease the collisional dissipation rate of fluctuation energy with respect to the ex-

pression of classic kinetic theory [20]. This has been taken into account by introducing a phenomenological correlation length in the classic expression of the collisional dissipation rate [21, 22] leading to what has been called Extended Kinetic Theory (EKT). More recently, it has been shown how particle friction is a factor in the dependence of both stresses and correlation length on volume fraction [23]. Finally, it has been suggested [24] how to include the role of finite particle stiffness, which affects the collision duration and allows for the development of rate-independent components of the stresses at solid volume fractions exceeding a critical value [25]. The aforementioned ingredients have enabled the applicability of kinetic theory even to dense flows.

EKT has been successfully tested against discrete numerical simulations of dry, simple shear flows [23, 24] and shearing flows between bumpy planes [26] and against physical experiments on dry, inclined flows over bumpy and erodible beds [27–30]. However, the latter comparisons were affected by the limited measurements attainable in physical experiments. For example, profiles of solid volume fraction and velocity fluctuations were not available; the flow interior, i.e., away from the sidewalls, where present, was not accessible.

In this paper we test EKT against numerical simulations using the Discrete Element Method (DEM) of steady, fully-developed, inclined granular flows over bumpy planes, in the presence or absence of flat, frictional sidewalls. We perform the simulations by changing the coefficient of normal restitution e_n (the negative of the ratio between the pre- and post-collisional normal relative velocity between two colliding spheres) and the angle of inclination of the bumpy plane and measure profiles of solid volume fraction, velocity, velocity fluctuations and stresses. We numerically solve the system of differential equations governing the flow, according to EKT, by making use of boundary conditions at the bumpy plane derived by Richman [31] for frictionless, nearly elastic spheres. Those boundary conditions underestimate the energy dissipation at the bumpy base for inelastic, frictional spheres: as a consequence, EKT predicts that steady and fully-developed flows are only possible below some critical value of the angle of inclination of the bumpy bottom, although we obtain steady and fully-developed DEM simulations also above this angle. We also show that, in the proximity of the bumpy plane, the relation between the pressure and the intensity of the velocity fluctuations (the granular temperature T) is affected by particle-boundary collisions [32]: ignoring this causes EKT to predict an increase of the solid volume fraction when approaching a dissipative boundary, in contrast with the DEM simulations, and to further underestimate the maximum angle of incli-

nation at which steady and fully-developed flows are possible. In the presence of flat, frictional sidewalls, we first prove that, when averaged along the spanwise direction, the ratio of the shear stress to the pressure linearly increases with the distance from the bottom plane, as often assumed [4,27,29,30], except for thin regions close to the free surface and the bottom. We obtain, from the slope of that linear relation, an effective wall friction coefficient which is much less than the actual friction coefficient of the particle-wall contacts and is independent of both the coefficient of normal restitution and the angle of inclination. We then use the effective wall friction to solve the differential equations of EKT by considering the average effect of the sidewalls on the flow and make comparisons with the spanwise averaged measurements in the numerical simulations. In addition to numerically solving the system of differential equations of EKT, we also obtain approximate analytical solutions with and without sidewalls, by assuming that the solid volume fraction is uniform throughout the flow. To do this we use the algebraic relation between the shear rate and the intensity of the velocity fluctuations which derives from the fluctuation energy balance when the divergence of the energy flux is neglected [27]. This latter approach is formally analogue to assuming a local rheology for the granular material which does not involve a measure of the particle velocity fluctuations.

The paper is organized as follows. In Sec. 2 we explain the simulation methodology. We then describe extended kinetic theory for inclined flows over a bumpy base in Sec. 3. Finally, we present the results of the simulations and the comparisons with the theory in Sec. 4, followed by conclusion remarks in Sec. 5.

2 Numerical simulations

As already mentioned, we have performed numerical simulations via Discrete Element Method (DEM). This a well-known tool in contact mechanics and many works [6,7,33,8] have previously used this approach for the study of granular flows. The simulations presented here were carried out using the open-source DEM software mercuryDPM [7,34]. This particular code has been validated against single-particle experiments [35] and compared in [7] against the previous DEM work of Silbert et. al. [6] where similar systems to those presented here were studied. An additional advantage of this code is that it offers a post processing tool to extract the continuum fields from numerical simulations via coarse-graining (CG). This technique has been used here to retrieve the field of interests for the comparisons with the results of extended kinetic theory (EKT). While

DEM and CG have been already presented elsewhere [36,37], we briefly introduce these methods in order to support our later discussions and comparisons.
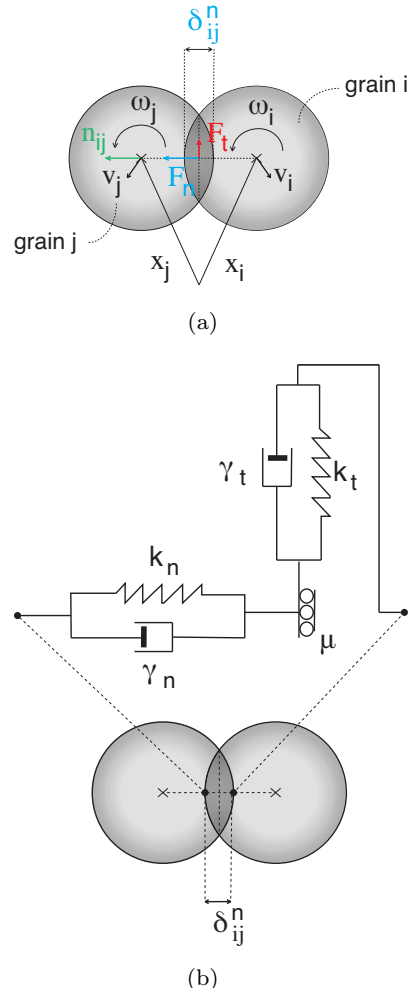

Fig. 1 Contact model: (a) two identical particles at contact; (b) sketch of the spring-dashpot model.

2.1 Contact model

In DEM, the material is treated as an ensemble of discrete particles, where every grain i is resolved as a Lagrangian point with position $\mathbf{x}_i$, mass m_i, velocity $\mathbf{v}_i$, moment of inertia I_i, and angular velocity $\boldsymbol{\omega}_i$. Considering a simple system of soft spherical particles of diameter d, contact forces are generated when particles interact with each other. This produces deformation to the particles which may be resolved via Hertz-Mindlin contact mechanics or similar. To simplify the contact behaviour, in this DEM code, interaction forces between rigid particles are related linearly by an

ideal particle overlap δ. This can be schematically visualized by considering a system where the interaction occurs between a pair of identical particles i, j (Fig. 1(a)). The two are in contact if $\delta^n > 0$, i.e., the normal overlap is positive. The overlap is easily defined as $\delta_{ij}^n = (d_i/2 + d_j/2) - (\mathbf{x}_i - \mathbf{x}_j) \cdot \mathbf{n}_{ij}$, where the normal contact vector $\mathbf{n}_{ij} = (\mathbf{x}_i - \mathbf{x}_j)/|\mathbf{x}_i - \mathbf{x}_j|$. It is assumed that the contact takes place at the centre of the overlap, a justifiable assumption as long as the overlap remains small.

The forces acting on particles i, j are determined using a standard spring-dashpot model (Fig. 1(b)). The same contact model is assumed in our simulations. Following this approach, the force acting from particle i to particle j can be decomposed into normal and tangential contributions, $\mathbf{F}_{ij} = \mathbf{F}_{ij}^n + \mathbf{F}_{ij}^t$. These are calculated in both normal and tangential directions as the combination of a linear repulsive and a linear dissipative components:

$$\mathbf{F}_{ij}^n = k_n \delta_{ij}^n - \gamma_n \mathbf{v}_{ij}^n;$$
$$\mathbf{F}_{ij}^t = -k_t \boldsymbol{\delta}_{ij}^t - \gamma_t \mathbf{v}_{ij}^t, \tag{1}$$

where, k_n and k_t are, respectively, the normal and tangential spring constants, γ_n and γ_t the normal and tangential viscous damping and the relative velocities in normal and tangential direction are defined as $\mathbf{v}_{ij}^n = (\mathbf{v}_{ij} \cdot \mathbf{n}_{ij})\mathbf{n}_{ij}$ and $\mathbf{v}_{ij}^t = \mathbf{v}_{ij} - \mathbf{v}_{ij}^n + \mathbf{l}_{ij} \times \boldsymbol{\omega}_i - \mathbf{l}_{ij} \times \boldsymbol{\omega}_j$. Here, the relative velocity of the pair is defined as $\mathbf{v}_{ij} = \mathbf{v}_i - \mathbf{v}_j$ and, for equal size particles, the vector $\mathbf{l}_{ij} = -(\mathbf{x}_i - \mathbf{x}_j)/2$.

It is straightforward to derive the collisional time t_c between two particles and the coefficient of normal restitution e_n from the normal component of the force as:

$$t_c = \pi / \left[k_n/m_{ij} - (\gamma_n/2m_{ij})^2 \right]^{1/2};$$
$$e_n = \exp(-t_c \gamma_n/(2m_{ij})), \tag{2}$$

where $m_{ij} = m_i m_j/(m_i - m_j)$ is the reduced mass (m_i and m_j being the masses of particles i and j, respectively).

The tangential component of the force is used to recreate the effect of particle surface roughness and to determine whether the particles stick or slide against one another. This effect is reproduced taking into account the generated force which is proportional to the elastic tangential displacement $\boldsymbol{\delta}_{ij}^t$. At the time of contact this is set to zero and its rate of change is given by [6,7]:

$$\frac{d\boldsymbol{\delta}_{ij}^t}{dt} = \mathbf{v}_{ij}^t - \frac{(\boldsymbol{\delta}_{ij}^t \cdot \mathbf{v}_{ij})\mathbf{n}_{ij}}{r_{ij}}. \tag{3}$$

Due to the possible rotation of the reference frame at the contact over time, the second term on the right hand side makes sure that the tangential displacement is always rotated: thus, at every time interval, it is kept tangential to the contact point. The magnitude of the tangential displacement is truncated to satisfy a yield criterion based on Coulomb's law, $|\mathbf{F}_{ij}^t| \leq \mu |\mathbf{F}_{ij}^n|$, where μ is the interparticle friction. Tangential sliding at a contact takes place when $|\mathbf{F}_{ij}^t| = \mu |\mathbf{F}_{ij}^n|$.

If all the contact forces $\mathbf{F}_i^c = \sum_{j=1, j \neq 1}^N \mathbf{F}_{ij}^c$ acting on the single particle i are known (e.g. from the contact with particles or the boundaries), its translational and rotational degrees of freedom can be solved by integrating Newton's equations of motion:

$$m_i \frac{d_2 \mathbf{x}_i}{dt_2} = \mathbf{F}_i^c + m_i \mathbf{g};$$
$$I_i \frac{d\boldsymbol{\omega}_i}{dt_2} = \mathbf{j}_i, \tag{4}$$

where $\mathbf{g}$ is the gravitational force (which here represents the only external force) and $\mathbf{j}_i = \sum_{j=1, j \neq 1}^N (\mathbf{l}_{ij} \times \mathbf{F}_{ij})$ is the total torque. Once the forces are known, these equations are a set of ordinary differential equations that can be solved numerically to update the particle positions at a chosen time step. The same process is performed for particle-wall interactions, with a new set of parameters (stiffness, dissipation and friction) that needs to be specified independently.

2.2 Coarse-graining

Coarse-graining is a technique used to simplify highly detailed and complex (anisotropic) microscopic quantities of heterogeneous materials and extract macroscopic continuum fields. The advantages of coarse-graining are that the equations of continuum mechanics are automatically satisfied, the particles can have different stiffness and shape and the results are even valid for a single time step, i.e. no ensemble-averaging is required [38]. The fields of interest in particle simulations are obtained by applying a local smoothing kernel (the coarse-graining function) characterized by a specific smoothing length (coarse-graining scale) denoted as w. A Gaussian defined with its standard deviation and scale (or variance) is a common example of a coarse-graining function. The scale, or resolution, is essential for obtaining correct measurements. Considering a general field, very fine resolutions (smaller than the particle scale) lead to strong fluctuations of the same field. However the value can plateau at a spatially dependent number and thereafter becomes independent of the scale. The plateaued value is what is usually referred to as the macroscopic field [39]. Narrower plateaus can also be found at large resolutions (larger than the particle scale) but they are strongly dependent on the field macroscopic gradients.

In explaining the procedure for coarse-graining, we consider velocity, solid volume fraction, granular temperature, stresses and kinetic energy flux. We take into consideration a system of N flowing particles while the particles fixed at the boundaries are labelled N_f.

The microscopic (point) mass density ρ^{mic}, at a point $\mathbf{r}$ and time t is defined from statistical mechanics as

$$\rho^{mic}(\mathbf{r}, t) = \sum_{i=1}^{N} m_i \Theta(\mathbf{r} - \mathbf{r}_i(t)), \tag{5}$$

where Θ is the Dirac delta function. The macroscopic mass density is calculated by convoluting the ρ^{mic} with a coarse-graining function $\psi(\mathbf{r})$:

$$\rho(\mathbf{r}, t) = \sum_{i=1}^{N} m_i \psi(\mathbf{r} - \mathbf{r}_i(t)). \tag{6}$$

Here, we assume the coarse-graining function to be a Gaussian:

$$\psi(\mathbf{r} - \mathbf{r}_i(t)) = \frac{1}{(\sqrt{2\pi}w)^3} \exp\left(-\frac{|\mathbf{r} - \mathbf{r}_i(t)|^2}{2w^2}\right) \tag{7}$$

with coarse-graining width w. The volume fraction ν is expressed as

$$\nu(\mathbf{r}, t) = \sum_{i=1}^{N} V\psi(\mathbf{r} - \mathbf{r}_i(t)), \tag{8}$$

where (for a sphere) $V = 1/6\pi d^3$ is the volume of the particle and ρ_p its density.

The flux of kinetic energy $\mathbf{q}(\mathbf{r}, t)$ is calculated as

$$\mathbf{q}(\mathbf{r}, t) = \frac{1}{2}\sum_{i=1}^{N} m_i \mathbf{v}_i \cdot \mathbf{v}_i \mathbf{v}_i \psi(\mathbf{r} - \mathbf{r}_i), \tag{9}$$

where $\mathbf{v}_i$ is the velocity of particle i.

Momentum density vector $\mathbf{M}(\mathbf{r}, t)$ is defined as:

$$\mathbf{M}(\mathbf{r}, t) = \sum_{i=1}^{N} m_i \mathbf{v}_i \psi(\mathbf{r} - \mathbf{r}_i). \tag{10}$$

The ratio of momentum to mass densities leads to the macroscopic velocity $\mathbf{V}(\mathbf{r}, t)$:

$$\mathbf{V}(\mathbf{r}, t) = \mathbf{M}(\mathbf{r}, t)/\rho(\mathbf{r}, t). \tag{11}$$

This allow to define the particle fluctuation velocity as:

$$\mathbf{C}_i(\mathbf{r}, t) = \mathbf{v}_i(t) - \mathbf{V}(\mathbf{r}, t). \tag{12}$$

The macroscopic stress can be obtained considering the momentum conservation equation [37]. This stress is subdivided into kinetic (i.e., streaming) and collisional stresses, $\boldsymbol{\sigma} = \boldsymbol{\sigma}^k + \boldsymbol{\sigma}^c$ whose explicit formulation reads:

$$\boldsymbol{\sigma}^k = \sum_{i=1}^{N} m_i \mathbf{C}_i \mathbf{C}_i \psi(\mathbf{x} - \mathbf{x}_i); \tag{13}$$

$$\boldsymbol{\sigma}^c = \sum_{i=1}^{N} \sum_{j=i+1}^{N} \mathbf{F}_{ij} \mathbf{x}_{ij} \int_0^1 \psi(\mathbf{r} - \mathbf{r}_i + s\mathbf{r}_{ij})ds$$
$$+ \sum_{i=1}^{N} \sum_{k=N+1}^{N+N_f} \mathbf{F}_{ik} \mathbf{a}_{ik} \int_0^1 \psi(\mathbf{r} - \mathbf{r}_i + s\mathbf{a}_{ij})ds, \tag{14}$$

with the interaction force between two particles $\mathbf{F}_{ij} = -\mathbf{F}_{ij}$, vectors $\mathbf{x}_{ij} = \mathbf{x}_i - \mathbf{x}_j$ and $\mathbf{a}_{ij} = \mathbf{x}_i - \mathbf{b}_{ij}$, where $\mathbf{b}_{ij}$ is the contact point between the particle i and a fixed wall particle j.

Once the stresses are known, the pressure, p, and the granular temperature, T, can be calculated as

$$p(\mathbf{x}, t) = tr(\boldsymbol{\sigma}(\mathbf{r}, t))/3 \tag{15}$$

and

$$T = tr(\boldsymbol{\sigma}^k)/3\rho, \tag{16}$$

respectively.

We remark that, for granular systems, the definition of the particle fluctuation velocity (Eq. 12) leads to scale dependency effects [37] due to gradients developing in the flow. For inclined flows, it has been suggested [37] that the scale dependency can be removed a posteriori from the kinetic stress $\boldsymbol{\sigma}^k$, which becomes:

$$\boldsymbol{\sigma}^{k\prime} = \sum_{i=1}^{N} m_i \mathbf{C}_i \mathbf{C}_i \psi(\mathbf{r} - \mathbf{r}_i) - \rho\dot{\gamma}^2 \frac{w^2}{3} \tag{17}$$

where $\dot{\gamma}$ is the shear rate. The same correction has been applied here, while the factor 3 appearing in the denominator in the right hand side expression is an integration constant [37].

Following the procedure described above, correct coarse-grained fields can be obtained near boundaries made of fixed particles (e.g. those at the bottom of the inclined chute). Other boundaries (e.g. lateral periodic or flat rigid walls) lead to local underestimations of these fields due to "vacuum" effects [40]. This happens when the coarse-graining function has to be partially defined beyond these boundaries. There are strategies to correct this, e.g. [40], but they are not implemented here. Instead, we disregard measurements taken within two diameters of the lateral boundaries. In considering these issues, it is striking to note that, usually, in physical experiments, the majority of available measurements for dry and opaque flowing materials are those taken close to the sidewalls, while the only reliable measurements in discrete element simulations are away from them.

2.3 Simulation methodology

We employ DEM to perform three-dimensional numerical simulations of granular systems flowing over a bumpy inclined plane in the absence and in the presence of flat, frictional sidewalls. In our reference coordinate system, x represents the streamwise (flow) direction, y the spanwise (vorticity) direction, and z is the direction perpendicular to the bed. We use three angles of inclination of the plane, i.e., $\theta = 24°$, $26°$ and $28°$. These values are within the range of possible inclinations that allow steady and fully-developed flows. The particles are identical spheres of diameter d and mass m which are subjected to the gravitational acceleration g.

To simulate flows in the absence of lateral confinement, we employ a simulation cell with lateral periodic boundaries along x and y. The system has dimension $l_x \times l_y = 20d \times 10d$. A single layer of 180 particles is glued at random spacing on the flat surface at $z = 0$ (so that their centres of mass are located at $z = d/2$). The average distance between the edges of two adjacent glued particles is $0.4d$. These particles cover the entire $x - y$ plain, although a few gaps are always present. These are generally filled during the simulations although particles trapped there are allowed to recirculate, i.e., are not fixed. All the simulations consist of 3500 flowing spherical particles which, within the simulation domain, can reach heights that are approximately $20d$.

When flat, frictional sidewalls are added, the domain is enlarged and periodic boundaries are used only along x (flow direction). The domain of simulation is $l_x \times l_y = 30d \times 66d$. The bumpy bottom is generated as described above, using 1760 particles so that the average distance between the edges of two adjacent particles is still $0.4d$ on average. A total of 27500 flowing spheres are simulated with typical heights of approximately $15d$.

For the contact model, we employ parameters similar to those used in other studies [6,37,8]. The constant particle stiffness in normal direction is $k_n = 2 \times 10^5 mg/d$. The damping γ_n is adjusted to obtain the desired value of the coefficient of normal restitution e_n. Here, results are given for e_n having values of 0.5, 0.6, and 0.7. The collisional time is $t_c = 0.005(d/g)^{1/2}$. For accurate simulations, a sufficiently small integration time step can then be defined as $\Delta t = t_c/50$ [6]. The tangential stiffness and damping are set as $k_t = 2/7k_n$ and $\gamma_t = 2/7\gamma_n$, respectively. All these parameters are used as inputs for both particle-particle and particle-flat wall collisions. Only the coefficient of sliding friction, μ, changes, being set 0.45 for particle-particle interactions and 0.35 for the particle-flat wall contacts.
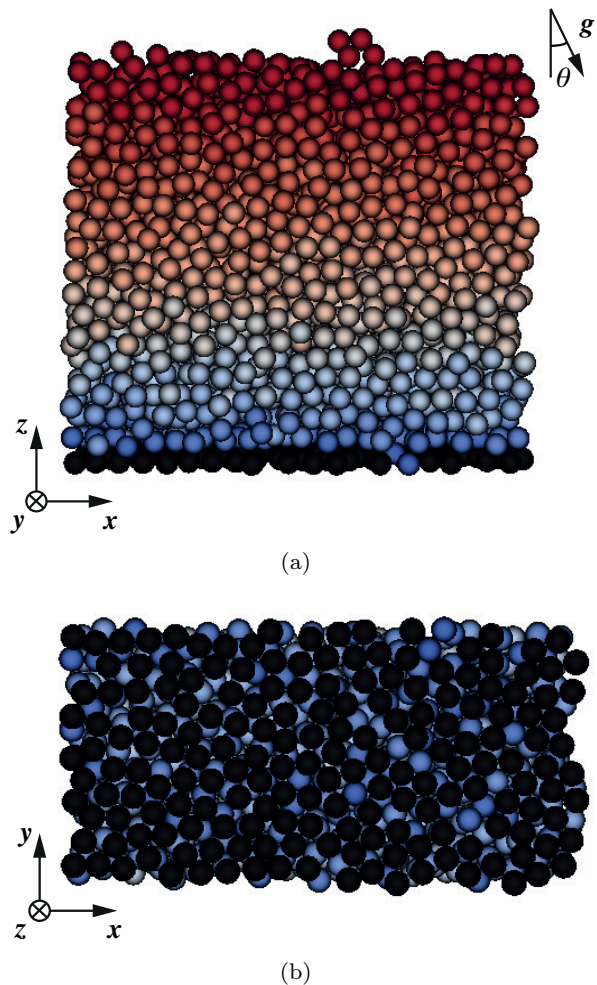

(a)

(b)

Fig. 2 Simulation cell with periodic boundaries of size $l_x \times l_y = 20d \times 10d$. A total of $N = 3500$ particles are simulated at different angles of inclination (θ). The side-view (a) shows the velocity gradient from slow (blue), at the bottom, to fast (red) particles, at the free-surface. The rough bottom base (b) is made by random placed particles (black) with centres at $z = d/2$.

Examples of snapshots of the DEM simulations obtained in the presence and in the absence of lateral confinement are reported in Fig. 2 and Fig. 3, respectively. At the beginning of the simulations, the bumpy plane is set horizontally and particles are randomly allocated within the simulation domain so that they do not overlap. Then, under the imposed force of gravity, particles settle until they form a packing. At this stage, the inclination is increased to give the particles enough energy to flow. Simulations are run until a steady state is reached. To verify this, as in [7], we check that the total kinetic energy of the system has reached a constant value over time. Steady flows can generally exist over a range of angles of inclination. For comparable simulation domains (at least in the absence of sidewalls), flow
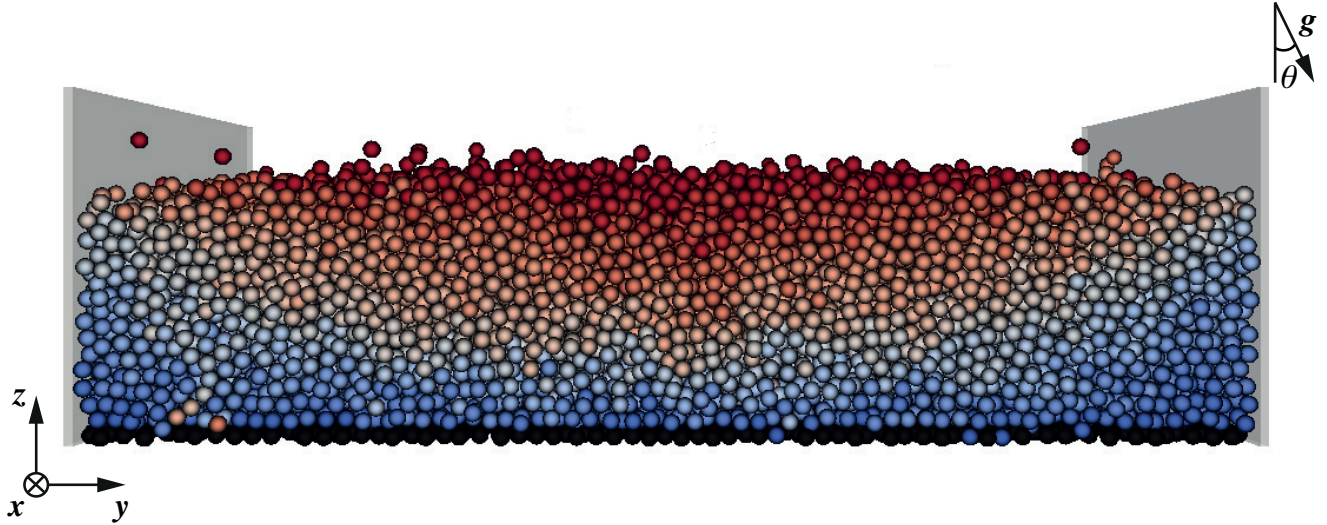
Fig. 3 Front view of a flow laterally confined by flat, rigid and frictional sidewalls. The simulation domain is $l_x \times l_y = 30d \times 66d$ with a total of $N = 27500$ particles simulated. As in Fig. 2, glued (black) particles make the base bumpy and the colour gradient represents slow (blue) to fast (red) particles as z increases. Notably, there is an additional influence of wall friction in the spanwise (y) velocity gradient.

heights and contact parameters, it has been shown in numerical simulations [7] that steady flows are possible between 21° and 29°. This observation motivated our choice of θ.

In the presence of lateral confinement, steady flows are possible also at angles of inclination greater than 29°, due to a well-known stabilizing effect of frictional sidewalls [10, 4]. Conversely, intermittent oscillations of kinetic energy and flow height were found to occur for values of the coefficient of normal restitution $e_n \geq 0.6$ at $\theta = 24°$. A similar behaviour was previously reported [41], although for different bottom roughness and slope angles.

Finally, coarse-graining is used to obtain the fields of interest and, after the steady state is reached, measurements are averaged over a time interval of $200(d/g)^{1/2}$ (longer time intervals do not alter the results).

3 Theory

In what follows, we assume that all quantities are averaged along the spanwise direction, with no change in notation for simplicity. Derivatives with respect to the z-direction are indicated with a prime. The spanwise averaged momentum balances along the z and x directions for steady and fully-developed inclined flows in the presence of sidewalls reduce to [27]:

$$p' = -\rho_p \nu g \cos \theta, \tag{18}$$

and

$$s' = -\rho_p \nu g \sin \theta + 2\frac{\mu_w}{l_y}p, \tag{19}$$

respectively, where s is the shear stress and μ_w is an effective wall friction coefficient, which accounts for the average force exerted by the sidewalls on the flow [4]. The expression for the sidewall force is just an approximation given that all particle-wall contacts are taken to be sliding and gradients in the velocity along the spanwise direction are ignored. We must emphasize that, in Eqs. (18) and (19), we have assumed that the normal stresses are isotropic and coincide with the pressure, although this is not strictly true for granular flows [42].

The balance of the fluctuation kinetic energy is

$$su' = Q' + \Gamma, \tag{20}$$

where u is the x-component of the particle velocity, Q is the fluctuation energy flux along z and Γ is the rate of collisional dissipation. The term on the left hand side of Eq. (20) represents the energy production through the work of the shear stress, while the divergence of the energy flux, Q', is the energy diffusion associated with the velocity fluctuations of the particles.

We use the constitutive relations for p, s, Q and Γ of kinetic theory [13, 26]

$$p = \rho_p f_1 T, \tag{21}$$

$$s = \rho_p d f_2 T^{1/2} u', \tag{22}$$

$$\Gamma = \rho_p \frac{f_3}{L} T^{3/2}, \qquad (23)$$

and

$$Q = -\rho_p d f_4 T^{1/2} T' - \rho_p d f_5 T^{3/2} \nu', \qquad (24)$$

where f_1, f_2, f_3, f_4 and f_5 are explicit functions of the volume fraction, the coefficient of normal restitution and the interparticle friction and are listed in Tab. 1. There, g_0 is the radial distribution function at contact, which accounts for two mechanisms: the increase in particle-particle collision probability due to excluded volume brought about by finite-size particles and its decrease due to shielding (binary encounters screened by other particles present along the colliding paths). [14]

Here, we use the expression suggested in [26] and valid for e_n less than or equal to 0.95:

$$g_0 = \frac{2 - \nu}{2 (1 - \nu)^3}, \qquad (25)$$

if $\nu \leq 0.4$; and

$$g_0 = \left[1 - \left(\frac{\nu - 0.4}{\nu_c - 0.4} \right)^2 \right] \frac{2 - \nu}{2 (1 - \nu)^3} + \left(\frac{\nu - 0.4}{\nu_c - 0.4} \right)^2 \frac{2}{\nu_c - \nu}, \qquad (26)$$

if $\nu > 0.4$.

In Eq. (26), ν_c represents the critical value of the solid volume fraction at which g_0 is singular for perfectly rigid spheres (i.e., the mean interparticle distance is zero along the principal compression axis, so that random aggregates of rigid particles develop a shear rigidity), which is only a function of surface friction [23].

Besides influencing the solid volume fraction at which g_0 diverges, surface friction also induces particle rotation. This would imply, in principle, the need to solve, in addition, rotational momentum and energy balances. A simplified approach consists of considering the transformation of translational kinetic energy into rotational kinetic energy as an additional loss for the former. As a consequence, an effective coefficient of restitution ϵ must be used in the function f_3 of Tab. 1 instead of e_n [18]. Numerical simulations [19] have provided a simple expression for the dependence of ϵ on e_n and μ:

$$\epsilon = e_n - \frac{3}{2} \mu \exp(-3\mu). \qquad (27)$$

In Eq. (23), L is the correlation length of extended kinetic theory, which decreases the rate of collisional dissipation due to the correlated motion of particles that occurs at solid volume fractions exceeding the freezing point [20,21,43]. When L is equal to one diameter, the molecular chaos assumption is valid and EKT

reduces to classic kinetic theory. Jenkins [21], using heuristic arguments, suggested to use

$$\frac{L}{d} = f_0 \frac{u'}{T^{1/2}}, \qquad (28)$$

where f_0 is a function of solid volume fraction, coefficient of normal restitution and surface friction (through ϵ) [22,23]:

$$f_0 = \left[\frac{2J}{15(1 - \epsilon^2)} \right]^{1/2} \times \left[\frac{26 (1 - \epsilon)}{15} \frac{\max(\nu - 0.49, 0)}{0.64 - \nu} + 1 \right]^{3/2}. \qquad (29)$$

We do not further complicate the theory by including the role of particle stiffness because this is relevant only at solid volume fractions close to ν_c [24] (i.e., $\nu_c \gtrsim 0.58$, where collisions cannot be considered instantaneous) and this does not occur in our numerical simulations (see later).

3.1 System of differential equations and boundary conditions

As in previous works [27,26], we can now write a system of differential equations that needs to be numerically integrated to solve for steady, fully-developed inclined flows.

Taking the derivative along z of Eq. (21), and using Eqs. (18) and (24), we obtain the equation governing the distribution of the solid volume fraction in the flow:

$$\nu' = \left(\frac{Q f_1}{\rho_p d f_4 T^{1/2}} - \nu g \cos \theta \right) \left[T \left(f_{1,\nu} - \frac{f_1 f_5}{f_4} \right) \right]^{-1}, \qquad (30)$$

where $f_{1,\nu}$ represents the derivative of f_1 with respect to ν.

The distribution of the shear stress is governed by Eq. (19), which reads, with Eq. (21),

$$s' = -\rho_p \nu g \sin \theta + 2 \rho_p \frac{\mu_w}{l_y} f_1 T. \qquad (31)$$

The distribution of the particle velocity is given by Eq. (22):

$$u' = \frac{s}{\rho_p d f_2 T^{1/2}}. \qquad (32)$$

Eq. (20), with Eqs. (32), (23) and (28), governs the distribution of the energy flux:

$$Q' = \frac{s^2}{\rho_p d f_2 T^{1/2}} - \frac{\rho_p^2 T^{5/2} f_2 f_3}{s d f_0}. \qquad (33)$$

Table 1 List of auxiliary coefficients in the constitutive relations of kinetic theory.

$$f_1 = 4\nu GF$$

$$f_2 = \frac{8J}{5\pi^{1/2}}\nu G$$

$$f_3 = \frac{12}{\pi^{1/2}}\left(1-\epsilon^2\right)\nu G$$

$$f_4 = \frac{4M\nu G}{\pi^{1/2}}$$

$$f_5 = \frac{25\pi^{1/2}N}{128\nu}$$

$$G = \nu g_0$$

$$F = \frac{1+e_n}{2}+\frac{1}{4G}$$

$$J = \frac{1+e_n}{2}+$$

$$\frac{\pi}{32}\frac{\left[5+2(1+e_n)(3e_n-1)G\right]\left[5+4(1+e_n)G\right]}{\left[24-6\left(1-e_n\right)^2-5(1-e_n^2)\right]G^2}$$

$$M = \frac{1+e_n}{2}+\frac{9\pi}{144\left(1+e_n\right)G^2}\times$$

$$\frac{\left[5+3G\left(2e_n-1\right)\left(1+e_n\right)^2\right]\left[5+6G\left(1+e_n\right)\right]}{16-7\left(1-e_n\right)}$$

$$N = \frac{96\nu\left(1-e_n\right)}{25G\left(1+e_n\right)}\frac{5+6G\left(1+e_n\right)}{16+3\left(1-e_n\right)}\times$$

$$\left\{\frac{20\nu H\left[5+3G\left(2e_n-1\right)\left(1+e_n\right)^2\right]}{48-21\left(1-e_n\right)}-\right.$$

$$\left. e_n\left(1+e_n\right)G\left(1+\nu H\right)\right\}$$

$$H = \frac{1}{G}\frac{\mathrm{d}G}{\mathrm{d}\nu}$$

The governing equation for the distribution of the granular temperature is given by Eq. (24), with Eq. (30):

$$T' = \left(-\frac{Q}{\rho_p df_4 T^{1/2}}+\frac{f_5\nu g\cos\theta}{f_{1,\nu}f_4}\right)\left(1-\frac{f_5}{f_{1,\nu}f_4}\right)^{-1}. \tag{34}$$

As in [27], the information about the number of particles in the system can be given in terms of the mass hold-up per unit basal area (the total mass of particles over unit area), $\mathcal{M}$. This can then be implemented as a boundary condition to a first order differential equation for the partial mass hold-up, $\mathrm{m}(z)=\int_0^z \rho_p\nu\mathrm{d}z$,

$$\mathrm{m}' = \rho_p\nu. \tag{35}$$

Boundary conditions need to be specified at the top and the bottom of the flow. We consider the top of the collisional flow to be located at $z=h$; we assume that, above h, the mean inter-particle distance is larger than the mean free path of kinetic theory, so that particles follow the free falling trajectories and particle-particle collisions can be neglected (ballistic layer). Pasini and Jenkins [44] determined the pressure at the interface with this ballistic layer, which gives, using the constitutive relation for the pressure in the dilute limit ($p=\rho_p\nu T$),

$$\rho_p\nu_t T_t = 0.039, \tag{36}$$

where, here and in what follows, the subscript t indicates that the quantity is evaluated at $z=h$ (top). At the interface with the ballistic layer (Fig. 4), the shear stress and the energy flux have been evaluated by Jenkins and Hanes [45] as

$$s_t = \rho_p\nu_t T_t\tan\theta \tag{37}$$

and

$$Q_t = -\rho_p\nu_t T_t^{3/2}\tan^2\theta, \tag{38}$$

respectively.

Richman [31] derived boundary conditions for the flow of spheres over a plane made bumpy by means of rigid, nearly elastic semi-spheres attached to it in a regular hexagonal fashion. Those boundary conditions apply at a distance of half a diameter from the top of the semi-spheres, i.e., at $z=1.5d$ in our configuration (where whole spheres are glued at the bottom). In what follows, the subscript b indicates that the quantity is evaluated at $z=1.5d$ (bottom). The slip velocity there results in

$$\frac{u_b}{T_b^{1/2}} = \left(\frac{\pi}{2}\right)^{1/2}\frac{s_b}{p_b}$$

$$\times\left[\frac{1}{3\sqrt{2}J_b}\frac{2^{3/2}J_b-5F_b\left(1+B\right)\sin^2\psi}{2\left(1-\cos\psi\right)/\sin^2\psi-\cos\psi}\right.$$

$$\left.+\frac{5F_b}{2^{1/2}J_b}\right], \tag{39}$$

where $B=\pi\left[1+5/\left(8G_b\right)\right]/\left(12\sqrt{2}\right)$, and J_b, F_b and G_b are obtained from the corresponding expressions of Tab. 1 with $\nu=\nu_b$. The boundary condition for the energy flux is [31]

$$Q_b = s_b u_b - \left(\frac{2}{\pi}\right)^{1/2}\frac{p_b T_b^{1/2}d}{L_b}(1-\epsilon)\frac{2\left(1-\cos\psi\right)}{\sin^2\psi}, \tag{40}$$

where, consistent with EKT, we have introduced the correlation length and the effective coefficient of restitution in the expression of the rate of collisional dissipation at the bumpy plane (second term on the right

hand side of Eq. (40)). In Eqs. (39) and (40), ξ measures the bumpiness of the base and is defined as $\sin \xi = (d + l)/(2d)$ where l is the distance between the edges of two adjacent spheres glued at the boundary [31]. Although ξ in Richman's boundary conditions refer to equally spaced semi-spheres attached in an hexagonal array, here we adopt the same definition by using, as l, the average distance between the edges of two adjacent spheres in our random configurations at the base. It is worth emphasizing that the analysis of Richman holds for $\pi/6 \leq \xi \leq \pi/3$: when $\xi = \pi/6$, the boundary particles are in close contact; while, when $\xi = \pi/3$, the flowing particles can fall, and therefore get trapped, in between two boundary particles.

Finally, we use the following boundary conditions for the partial mass hold-up:

$$\mathrm{m}_b = 0, \tag{41}$$

and

$$\mathrm{m}_t = \mathcal{M}. \tag{42}$$

We solve the system of six differential equations (30) through (35) in the six unknowns ν, s, u, Q, T and m using the Matlab 'bvp4c' two-point boundary value problem solver with the seven boundary conditions, (36) through (42). The additional boundary condition allows the value of h to be determined.

3.2 Algebraic and incompressible approximation

A simplified approach to the solution of inclined, dense, granular flows consists of assuming that the solid volume fraction is constant within the flow and that the divergence of the energy flux in the fluctuation energy balance (Eq. (20)) is negligible. The latter assumption implies, from Eq. (20) with Eqs. (22), (23) and (28),

$$\frac{du'}{T^{1/2}} = \left(\frac{f_3}{f_2 f_0}\right)^{1/3}, \tag{43}$$

i.e., that there is a one-to-one algebraic relation between the shear rate and the square root of the granular temperature. The granular temperature is therefore enslaved to u' and it is no longer an independent quantity in the problem. The algebraic assumption makes the constitutive relations of EKT formally analogue to the phenomenological local rheology based on the inertial parameter [15,4], with the advantage that, unlike the latter, there are no parameters that need to be fitted against experiments.

In the dense limit, i.e., by retaining only terms proportional to G in the expressions of Tab. 1, the ratio of

s over p can be expressed, using Eqs. (22), (21), (43) and (29), as

$$\frac{s}{p} = \left[\frac{6(1 - \epsilon^2)J}{5\pi F^2}\right]^{1/2} \left[\frac{26(1 - \epsilon)}{15} \frac{\nu - 0.49}{\nu_c - \nu} + 1\right]^{-1/2}, \tag{44}$$

where J and F are now only functions of e_n. If we take the stress ratio to be roughly equal to $\tan \theta$ (this is strictly true only in the absence of sidewalls), and invert Eq. (44), we obtain the relationship between the solid volume fraction varies and the slope of the channel:

$$\nu = \left[\frac{26(1 - \epsilon)}{15} 0.49 + \frac{6(1 - \epsilon^2)J}{5\pi F^2 \tan^2 \theta} \nu_c - \nu_c\right]$$
$$\times \left[\frac{26(1 - \epsilon)}{15} + \frac{6(1 - \epsilon^2)J}{5\pi F^2 \tan^2 \theta} - 1\right]^{-1}. \tag{45}$$

If the mass hold-up $\mathcal{M}$ is given, the height of the flow can then be calculated as $h = \mathcal{M}/(\rho_p \nu)$.

The integration of Eqs. (18) and (19), with ν uniform and neglecting the stresses at $z = h$, gives

$$p = \rho_p \nu g (h - z) \cos \theta, \tag{46}$$

and

$$s = \rho_p \nu g (h - z) \sin \theta - \frac{\mu_w}{l_y} \rho_p \nu g (h - z)^2 \cos \theta, \tag{47}$$

respectively.

From Eqs. (21) and (46) and the expression of f_1 in Tab. 1, the granular temperature is linearly distributed along z,

$$T = \frac{1}{4FG} g (h - z) \cos \theta. \tag{48}$$

From the constitutive relations for the shear stress and the pressure (Tab. 1), we obtain

$$u' = \frac{5\pi^{1/2} F}{2J} \frac{s}{p} \frac{T^{1/2}}{d}. \tag{49}$$

Using Eqs. (46), (47) and (48) in Eq. (49) and integrating gives

$$u = u_b + \left(\frac{25\pi g F \cos \theta}{16 G J^2 d^2}\right)^{1/2}$$
$$\times \left\{\frac{2}{3} \tan \theta \left[h^{3/2} - (h - z)^{3/2}\right]\right.$$
$$\left. - \frac{2}{5} \frac{\mu_w}{l_y} \tan \theta \left[h^{5/2} - (h - z)^{5/2}\right]\right\}, \tag{50}$$

where u_b is given in Eq. (39).

4 Results and discussions

Here we show and discuss the comparisons between the results of DEM simulations, the numerical solutions of EKT obtained from the integration of the full system of differential equations (Sec. 3.1) and the approximate analytical solutions of EKT for the hypothesis of incompressible, algebraic flow (Sec. 3.2).

As discussed, we performed the DEM simulations at three angles of inclination ($\theta = 24°$, $26°$ and $28°$), using three values of the coefficient of normal restitution, $e_n = 0.5$, 0.6 and 0.7, and keeping constant the value of the particle-particle friction $\mu = 0.45$. From Eq. (27), then, the corresponding effective coefficients of restitution in the expressions of the collisional dissipation rate and the correlation length of EKT are $\epsilon = 0.325$, 0.425 and 0.525, respectively. From the dependence of the solid volume fraction at shear rigidity on interparticle friction given in [23], we obtain $\nu_c = 0.59$. Furthermore, from the average distance between the edges of two adjacent spheres glued at the bottom plane of the DEM simulations in the formula for the bumpiness, we set $\xi = 0.78$ in the expressions of Richman [31] for the boundary conditions. Finally, the profiles of particle pressure p obtained from DEM simulations showed linear (hydrostatic) profiles in all cases, with values that increased with depth. For this reason, they are not presented here.

For clarity, we depict in Fig. 4 a typical side-view of a DEM simulation in which we have identified the different layers we have already mentioned or we will mention in the following.

4.1 Inclined flows without sidewalls

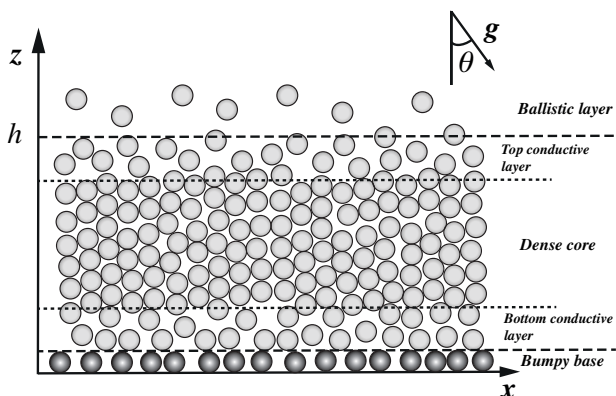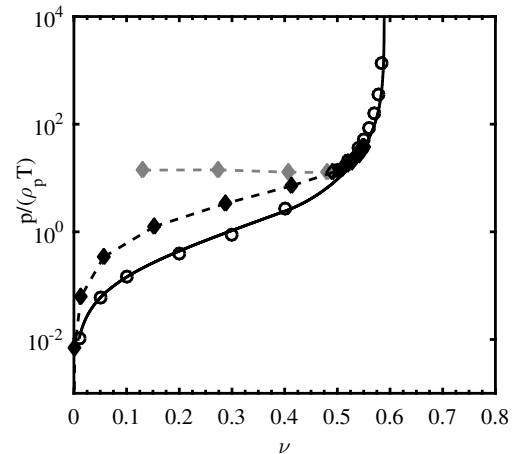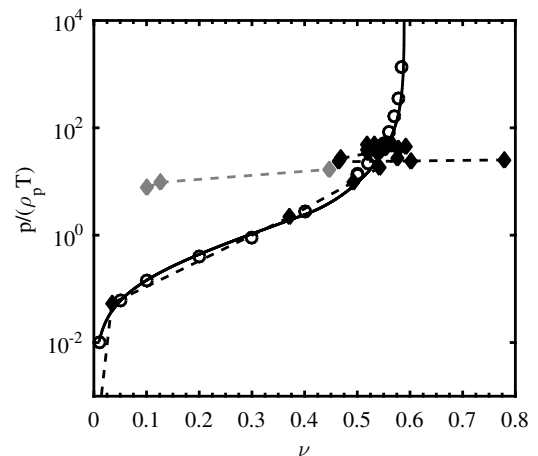We carried out the DEM simulations on inclined flows in the absence of lateral confinement using 3500 parti-

Fig. 4 Different layers in the flow domain.

(a)

(b)

Fig. 5 Dimensionless pressure (diamonds and dashed lines) versus solid volume fraction obtained from a DEM simulation of inclined flow in the absence of sidewalls when $e_n = 0.7$, $\mu = 0.45$ and $\theta = 26°$ for two smoothing lengths: (a) $w = 1d$ and (b) $w = 0.1d$. Grey diamonds and dashed lines refer to measurements within three diameters of the bottom. The solid line represents Eq. (21). Also shown are the results of DEM simulations of simple shearing with $e_n = 0.7$ and $\mu = 0.5$ (circles, after [19]).

cles on a basal area of $200d^2$. This implies that the mass hold-up was $\mathcal{M} = 3500(\rho_p \pi d^3/6)/(200d^2) = 9.16\rho_p d$.

We first check that the constitutive relations of kinetic theory are suitable to describe inclined granular flows by comparing the dimensionless pressure $p/(\rho_p T)$ against the solid volume fraction measured in the DEM simulations when $e_n = 0.7$ and $\theta = 26°$ with the theoretical predictions of Eq. (21) (the following analysis holds also for different values of e_n and θ, not shown here for clarity).

If we employ a smoothing length $w = 1d$ in the coarse-graining procedure (Fig. 5a), and we use Eq. (17)

to eliminate the scale dependency from both the pressure and the granular temperature, we notice that the numerical results are characterized by two branches for solid volume fractions less than approximately 0.5. We anticipate that ν is less than 0.5 in two layers, one close to the bumpy bottom and one close to the top ballistic layer. In these layers, the divergence of the energy flux cannot be neglected in the energy balance and thus we term them conductive layers (Fig. 4). The theoretical curve of kinetic theory predicts that the dimensionless pressure increases when the solid volume fraction increases. The lower branch of the numerical results (measurements obtained in the proximity of the ballistic layer) follows the theory at least qualitatively, while the upper branch (which comprises measurements in a region within three diameters of the bottom plane) slightly decreases for increasing ν. For ν greater than 0.5 (the dense core region of the inclined flow), the numerical measurements collapse onto the theoretical curve. Fig. 5a shows also the numerical results obtained in DEM simulations of simple shearing (i.e., uniform shear rate) for the same coefficient of normal restitution and slightly larger friction coefficient [19], which are in excellent agreement with Eq. (21). This means that the the lack of agreement of our DEM with EKT shown in Fig. 5a has to do with the spatial variation of the velocity gradient.

If we reduce the smoothing length to $w = 0.1d$ (Fig. 5b), we observe that there is a scattering of the measurements around the theoretical curve due to layering of particles in organized rows [37]: solid volume fractions well beyond ν_c (as large as 0.8) are now possible. On the other hand, the measurements at the top of the flow, which belonged to the lower branch of Fig. 5a, are now well fitted by Eq. (21). This indicates that there is a residual, but substantial, scale-dependency of the measurements on the smoothing length that cannot be simply corrected through Eq. (17). The measurements at the bottom of the flow still completely disagree with Eq. (21) (grey symbols in Fig. 5b). This might be due to the fact that the radial distribution function at contact in Eq. (21) only takes into account excluded volume and shielding in particle-particle interactions, while there are analogous mechanisms involved in particle-boundary interactions [32]. Defining a radial distribution function at contact in the proximity of solid boundaries is still an open question (some efforts have been made to determine g_0 in the proximity of frictional, flat walls [47]) since g_0 is generally only well defined [14,46] for a general element volume where the particles sufficiently far from them. We will see later what are the implications of using an incorrect g_0 near to such boundaries.
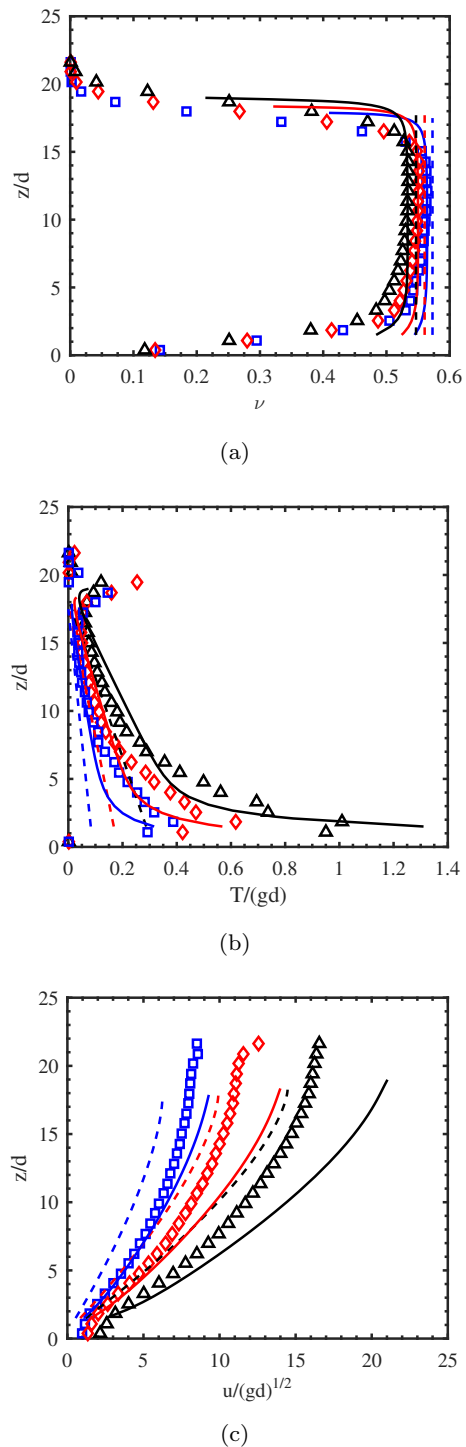

(a)

(b)

(c)

Fig. 6 Numerical (symbols) profiles of (a) solid volume fraction, (b) dimensionless granular temperature and (c) dimensionless particle velocity obtained from DEM simulations of inclined flows in the absence of sidewalls when $e_n = 0.5$, $\mu = 0.45$ and $\theta = 24°$ (squares), $\theta = 26°$ (diamonds) and $\theta = 28°$ (triangles). Solid and dashed lines represent the results of the numerical integration of the full system of differential equations of EKT and its incompressible, algebraic approximation, respectively.
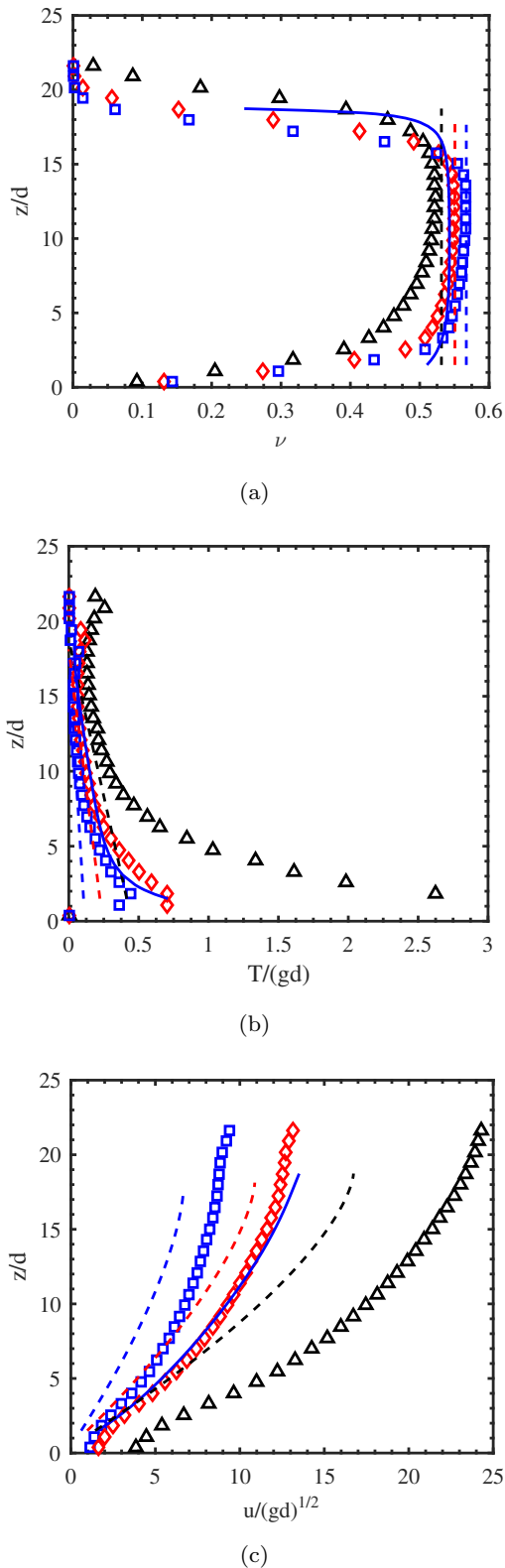
(a)

(b)

(c)

Fig. 7 Same as in Fig. 6, but when $e_n = 0.7$. Solid lines refer to the case $\theta = 24°$ only (no solution was possible for larger angles of inclination of the bottom.)

From Figs. 6 to 8, we show the comparisons between the results of the DEM simulations in the absence of sidewalls and the predictions of EKT, in terms of profiles of solid volume fraction, velocity and granular temperature. In what follows, we employ $w = 1d$ to coarse-grain the profiles of solid volume fraction and velocity from DEM simulations and $w = 0.1d$ to coarse-grain profiles of granular temperature (to further eliminate the scale-dependency).

Fig. 6 shows results for $e_n = 0.5$, at the three slope inclinations simulated. Fig. 6a confirms that inclined flows over rough surfaces in the absence of sidewalls are characterized by two regions, one at the top and one at the bottom, where the flow is more dilute and a core region where the flow is dense (Fig. 4). The numerical solution of the full system of differential equations of EKT satisfactorily reproduces this feature, unlike, evidently, its incompressible, algebraic approximation. The numerical solution of EKT can also reproduce the greater than linear increase of the granular temperature in those two dilute regions when approaching the ballistic layer and the bumpy bottom (Fig. 6b); while the incompressible, algebraic approximation simply predicts a linear decrease of T with z (Eq. (48)). Finally, the numerical solutions of EKT overestimate the velocities in the upper part of the flow, while the incompressible algebraic approximation underestimate them (Fig. 6c). The numerical solutions of EKT overestimate the velocities due to the fact that the viscosity, whose expression does not take into account the role of friction (Eq. (22) and Tab. 1), is underestimated [19]. This emphasizes the need for a better understanding of the influence of friction on the shear stress.

Similar considerations apply also to the case $e_n = 0.7$ (Fig. 7), but with a crucial difference: in this case, numerical solutions of the full system of differential equations of EKT of Sec. 3.1 are possible only up to angles of inclination slightly above $24°$. In other words, steady, fully-developed flows cannot be sustained at larger angles, and the theory predicts that the flow would continue to accelerate along the plane. The fact that the incompressible, algebraic approximation does not present the same limitation indicates the crucial role of the boundaries in controlling the maximum angle for which steady, fully-developed flows are possible.

The maximum angle of inclination that allows steady, fully-developed flows is underestimated in the EKT. It is possible that this is due to the underestimation of dissipation at the bumpy bottom, as imposed by the boundary conditions of Richman [31]. To verify this, we now measure the values of $u = 2.26(gd)^{1/2}$ and $Q = -0.13\rho_p(gd)^{3/2}$ at $z = 1.5d$ in the DEM simulation with $e_n = 0.7$ and $\theta = 26°$ and directly employ those as
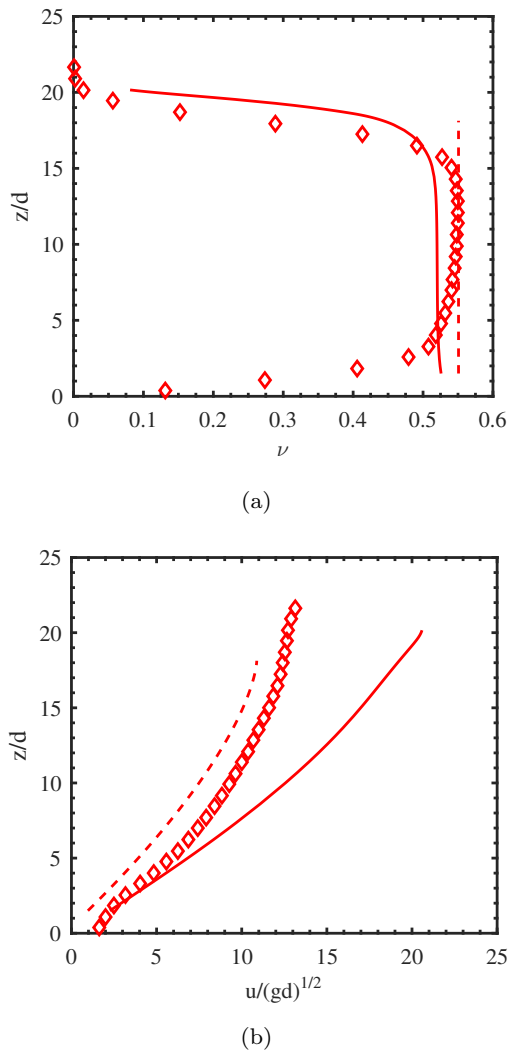
(a)

(b)

Fig. 8 Numerical (diamonds) profiles of (a) solid volume fraction and (b) dimensionless particle velocity obtained from the DEM simulation of inclined flow in the absence of sidewalls when $e_n = 0.7$, $\mu = 0.45$ and $\theta = 26°$. The solid lines represent the results of the numerical integration of the full system of differential equations of EKT when the boundary conditions at the bottom are those measured in the DEM simulation. The dashed lines are the results of the incompressible, algebraic approximation of EKT.

boundary conditions for solving the corresponding differential problem of EKT. Fig. 8 shows that the modification of the boundary conditions at the bottom is indeed sufficient to obtain a solution for $\theta = 26°$ (previously forbidden). However, the negative value of the fluctuation energy flux, which indicates the dissipative nature of the bumpy bed in the DEM simulation, induces an increase of the solid volume fraction near the bottom, in contrast to the DEM results (Fig. 8a). If we increase the energy dissipation at the bottom, we will cause a further increase of the solid volume fraction there, that eventually will approach the singular value
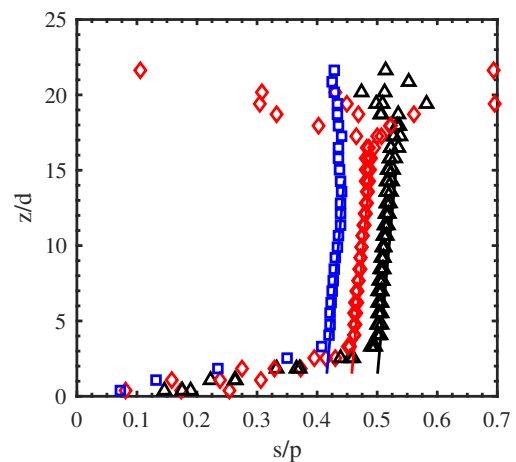

Fig. 9 Spanwise averaged profiles of stress ratio (symbols) along the flow obtained from DEM simulations of inclined flows in the presence of sidewalls for all coefficients of restitution with $\mu = 0.45$ and $\theta = 24°$ (squares), $\theta = 26°$ (diamonds) and $\theta = 28°$ (triangles). Solid lines represent Eq. (51).

ν_c and prevent a numerical solution to the differential equations from being obtained. For this reason, even if we take the boundary conditions from the DEM simulations, we are unable to find steady and fully-developed solutions to the flow for θ larger than 26°. This indicates also that the adoption of more sophisticated boundary conditions that include the role of friction in a more rigorous way [48] and/or nonlinear terms in the ratio of slip velocity to the square root of the granular temperature [32] would not solve this discrepancy. As discussed, this may relate to issues with the radial distribution function at contact near the bottom (Fig. 5). It is likely that modifying g_0 to take into account the influence of the boundary would allow EKT to predict a decrease of the solid volume fraction when approaching the dissipative bottom, as in the DEM simulations.

4.2 Inclined flows with sidewalls

We also performed DEM simulations on inclined flows in the presence of flat, frictional sidewalls using 27500 particles on a basal area of $1980d^2$, so that the mass hold-up was $\mathcal{M} = 7.27\rho_p d$. The sliding friction coefficient of particles in contact with the sidewalls was set equal to 0.35.

If we take the ratio of Eq. (47) to Eq. (46), we obtain

$$\frac{s}{p} = \tan\theta - \frac{\mu_w}{l_y}(h - z), \tag{51}$$

i.e., the stress ratio linearly decreases when moving from the free surface to the bottom of the flow. This approximate relation explains why frictional sidewalls

allow for steady and fully-developed flows over erodible beds at angles of inclination that are much larger than the angle of repose of the granular material. [10] Eq. (51) has been widely used in analytically solving for laterally confined surface flows [4,27,29,30]. The advantage is that one can transform two-dimensional into one-dimensional flows by simply taking into account the average resistance of the sidewalls. It is not clear whether Eq. (51) is able to accurately represent the distribution of mean stress ratio along the flow, however. To verify this, we plot the spanwise averaged profiles of stress ratio for the three angles of inclination in Fig. 9. In the core region of the flows, where the solid volume fraction (Fig. 10a) is approximately constant (the assumption behind Eq. (51)), the stress ratio is indeed linearly distributed, with a slope which is independent of both θ and e_n. By fitting the results of the numerical simulations, we obtain $\mu_w = 0.15$: the effective wall friction coefficient is much less than the actual value of the sliding friction for the particle-flat wall interaction, 0.35. This might relate to the fact that only some of the contacts at the wall are actually sliding while part are rolling, thus decreasing μ_w. The value $\mu_w = 0.15$ is then used in both the full system of differential equations of EKT and its incompressible, algebraic approximation and the results are shown in Fig. 10.

Fig. 10 demonstrates that the quantitative agreement between EKT and the DEM results for $e_n = 0.5$ is improved when flat, frictional sidewalls are present. However, as in the case without sidewalls, the maximum angle of inclination for having steady and fully-developed flows is still underestimated for the other values of the coefficient of normal restitution (not shown here for brevity) due to the incorrect radial distribution function at contact near the bumpy base.

5 Conclusion

We have performed DEM simulations of steady and fully-developed, inclined flows of inelastic, monosized spheres over bumpy bases in the absence and in the presence of flat, frictional sidewalls and made comparisons with the predictions of extended kinetic theory, i.e., kinetic theory of granular gases modified to take into account the role of interparticle friction in collisions and the correlation in velocity fluctuations at solid volume fractions exceeding the freezing point. We have transformed the constitutive relations of EKT and momentum and energy balances into a set of differential equations that we have solved numerically to find distributions of stresses, velocity, solid volume fraction and granular temperature. Analytical solutions have been also obtained for the assumptions of incompressibility
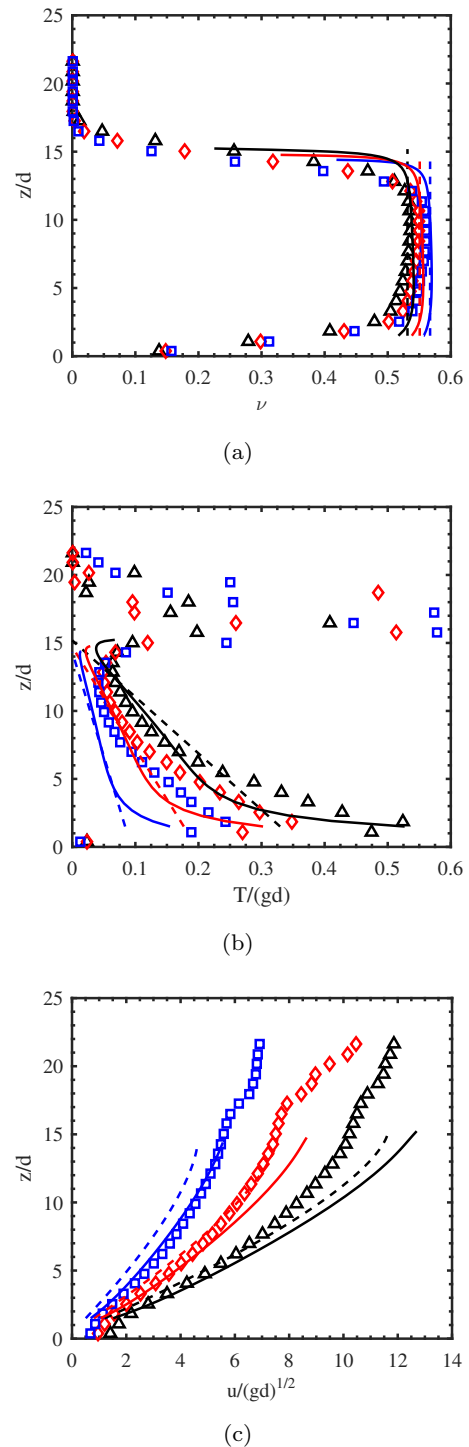

(a)

(b)

(c)

Fig. 10 Numerical (symbols) spanwise averaged profiles of (a) solid volume fraction, (b) dimensionless granular temperature and (c) dimensionless particle velocity obtained from DEM simulations of inclined flows in the presence of sidewalls when $e_n = 0.5$, $\mu = 0.45$ and $\theta = 24°$ (squares), $\theta = 26°$ (diamonds) and $\theta = 28°$ (triangles). Solid and dashed lines represent the results of the numerical integration of the full system of differential equations of EKT and its incompressible, algebraic approximation, respectively.

and algebraic balance between the work of the shear stress and the energy dissipated in collisions. The results of DEM simulations have been coarse-grained and we have confirmed that there is a scale-dependency of the stresses that can be removed if the smoothing length in the coarse-graining is taken to be one tenth of the particle diameter (other suggestions from the literature to remove the scale-dependency did not work). After the removal of the scale-dependency, the constitutive relation for the pressure of kinetic theory is in excellent agreement with the numerical results, but for a region of a few diameters close to the bumpy base where the particle-boundary collisions affect the radial distribution function at contact g_0. We have suggested that the most crucial consequence of an incorrect choice of g_0 in the proximity of the boundary is a substantial underestimation by EKT of the range of angles of inclination of the base for which steady and fully-developed flows are possible. We have also shown that the current state of the art of the boundary conditions for kinetic theory applied at a bumpy bottom underestimates the energy dissipation there. Besides the above mentioned limitations that need to be addressed in future works, extended kinetic theory (even its incompressible, algebraic approximation) agrees well with the DEM results in the absence of sidewalls (i.e. one-dimensional flow). In the presence of sidewalls, the flow becomes two-dimensional. We have demonstrated though, as previously suggested, that the spanwise averaged ratio of shear stress to pressure linearly decreases with the distance from the free surface, in accordance with the approximation of considering the sidewalls as providing a Coulomb-like resistance to the flow. The effective Coulomb friction coefficient is found to be less than half the actual value of the friction coefficient of the particles with the flat wall. Using this effective friction coefficient allows extended kinetic theory to agree with the DEM results even in the presence of the sidewalls.

The authors declare that they have no conflict of interest.

References

1. Azanza, E., Chevoir, F., Moucheront, P., Experimental study of collisional granular flows down an inclined plane. Journal of Fluid Mechanics 400, 199-227 (1999)
2. Pouliquen, O., Scaling laws in granular flows down rough inclined planes. Physics of Fluids 11(3), 542-548 (1999)
3. Louge, M.Y., Keast, S.C., On dense granular flows down flat frictional inclines. Physics of Fluids 13(5), 1213-1233 (2001)
4. Jop, P., Forterre, Y., Pouliquen, O., Crucial role of sidewalls in granular surface flows: consequences for the rheology. Journal of Fluid Mechanics 541, 167-192 (2005)
5. Hanes, D.M., Walton, O.R., Simulations and physical measurements of glass spheres flowing down a bumpy incline, Powder Technology, 109(1-3), 133-144 (2000)
6. Silbert, L.E., Ertas, D., Grest, G.S., Halsey, T.C., Levine, D., Plimpton, S.J., Granular flow down an inclined plane: Bagnold scaling and rheology. Physical Review E 64(5), 051302 (2000)
7. Weinhart, T., Thornton, A.R., Luding, S., Bokhove, O., Closure relations for shallow granular flows from particle simulations. Granular Matter 14(4), 531-552 (2012)
8. Brodu, N., Delannay, R., Valance, A., Richard, P., New patterns in high-speed granular flows, Journal of Fluid Mechanics, 769, 218-228 (2015)
9. Delannay, R., Louge, M., Richard, P., Taberlet,N., Valance, A., Towards a theoretical picture of dense granular flows down inclines. Nature Materials 27, 99108 (2007)
10. Taberlet, N., Richard, P., Henry, E., Delannay, R., The growth of a Super Stable Heap: An experimental and numerical study. EPL (Europhysics Letters) 68(4), 515 (2004)
11. Jenkins, J.T., Savage, S.B., A theory for the rapid flow of identical, smooth, nearly elastic, spherical particles. Journal of Fluid Mechanics 130, 187-202 (1983)
12. Lun, C.,K.,K., Kinetic theory for granular flow of dense, slightly inelastic, slightly rough spheres. Journal of Fluid Mechanics 233, 539-559 (1991)
13. Garzó, V., Dufty, J.W., Dense fluid transport for inelastic hard spheres. Physical Review E 59(5), 5895–5911 (1999)
14. Torquato, S., Nearest-neighbour statistics for packing of hard spheres and disks. Physical Review E 51, 3170 (1995)
15. GDR MiDi, On dense granular flows. The European Physical Journal E 14(4), 341-365 (2004)
16. Kamrin, K., Koval, G., Nonlocal Constitutive Relation for Steady Granular Flow. Physical Review Letters 108(17), 178301 (2012)
17. Forterre, Y., Pouliquen, O. Flows of Dense Granular Media. Annual Review of Fluid Mechanics 40(1), 1-24 (2008)
18. Jenkins, J.T., Zhang, C., Kinetic theory for identical, frictional, nearly elastic spheres, Physics of Fluids, 14(3), 1228-1235 (2002)
19. Chialvo, S., Sundaresan, S., A modified kinetic theory for frictional granular flows in dense and dilute regimes. Physics of Fluids 25(7), 070603 (2013)
20. Mitarai, N., Nakanishi, H., Velocity correlations in dense granular shear flows: Effects on energy dissipation and normal stress. Physical Review Letters 75(3), 031305 (2007)
21. Jenkins, J.T., Dense inclined flows of inelastic spheres, Granular Matter, 10(1), 47-52 (2007)
22. Berzi, D., Extended kinetic theory applied to dense, granular, simple shear flows. Acta Mechanica 225(8), 2191-2198 (2014)
23. Berzi, D., Vescovi, D., Different singularities in the functions of extended kinetic theory at the origin of the yield stress in granular flows. Physics of Fluids 27(1), 013302 (2015)
24. Berzi, D., Jenkins, J.T., Steady shearing flows of deformable, inelastic spheres. Soft Matter 11(14), 4799-4808 (2015)
25. Chialvo, S., Sun, J., Sundaresan, S., Bridging the rheology of granular flows in three regimes. Physical Review Letters 85(2), 021305 (2012)

26. Vescovi, D., Berzi, D., Richard, P., Brodu, N., Plane shear flows of frictionless spheres: Kinetic theory and 3D soft-sphere discrete element method simulations. Physics of Fluids 26(5), 053305 (2014)

27. Jenkins, J.T., Berzi, D., Dense inclined flows of inelastic spheres: tests of an extension of kinetic theory, Granular Matter, 12(2), 151-158 (2010)

28. Jenkins, J.T., A Chute Flow of Inelastic Spheres, Progress of Theoretical Physics Supplement, 184, 49 (2010)

29. Berzi, D., Jenkins, J.T., Surface flows of inelastic spheres. Physics of Fluids 23(1), 013303 (2011)

30. Jenkins, J.T., Berzi, D., Kinetic theory applied to inclined flows. Granular Matter 14(2), 79-84 (2012)

31. Richman, M.W., Boundary conditions based upon a modified Maxwellian velocity distribution for flows of identical, smooth, nearly elastic spheres. Acta Mechanica 75(1), 227-240 (1988)

32. Xu, H., Louge, M., Reeves, A., Solutions of the kinetic theory for bounded collisional granular flows. Continuum Mechanics and Thermodynamics 15(4), 321-349 (2003)

33. Thornton, A.R., Weinhart, T., Luding, S., Bokhove, O., Frictional dependence of shallow-granular flows from discrete particle simulations. The European Physical Journal E 35(12), 127 (2012)

34. www.mercurydpm.org

35. Fuchs, R, Weinhart, T., Meyer, J., Zhuang, H., Staedler, T., Jiang, X., Luding, S., Rolling, sliding and torsion of micron-sized silica particles: experimental, numerical and theoretical analysis. Granular Matter 16(3), 281-297 (2014)

36. Luding, S., Introduction to discrete element methods. European Journal of Environmental and Civil Engineering 12(7-8), 785-826 (2008)

37. Weinhart, T., Hartkamp, R., Thornton, A.R., Luding, S., Coarse-grained local and objective continuum description of three-dimensional granular flows down an inclined surface. Physics of Fluids 125(7), 070605 (2013)

38. Tunuguntla, D. R., Thornton, A.R., Weinhart, T., From discrete elements to continuum fields: Extension to bidisperse systems. Computational Particle Mechanics 3(3), 349-365 (2016)

39. Goldhirsch, I., Stress, stress asymmetry and couple stress: from discrete particles to continuous fields. Granular Matter 12(3), 239-252 (2010)

40. Ries, A., Brendel, L., Wolf, D.E., Coarse graining strategies at walls. Computational Particle Mechanics 1(2), 177-190 (2014)

41. Silbert, L.E., Grest, G.S., Plimpton, S.J., Levine, D., Boundary effects and self-organization in dense granular flows. Physics of Fluids 14(8), 2637-2646 (2002)

42. Saha, S., Alam, M., Normal Stress Differences, Their Origin and Constitutive Relations for a Sheared Granular Fluid. Journal of Fluid Mechanics 795, 549-580 (2016)

43. Kumaran, V., Dynamics of dense sheared granular flows. Part II. The relative velocity distributions. Journal of Fluid Mechanics 632, 145-198 (2009)

44. Pasini, J.M., Jenkins, J.T., Aeolian transport with collisional suspension. Philosophical Transactions of the Royal Society of London A: Mathematical, Physical and Engineering Sciences 363(1832), 1625-1646 (2005)

45. Jenkins, J.T., Hanes, D.M., The balance of momentum and energy at an interface between colliding and freely flying grains in a rapid granular flow. Physics of Fluids A: Fluid Dynamics 5(3), 781-783 (1993)

46. Carnahan, N.F., Starling, K.E., Equation of State for Non-attracting Rigid Spheres. The Journal of Chemical Physics 51(2), 635-636 (1969)

47. Louge, M.Y., Computer simulations of rapid granular flows of spheres interacting with a flat, fractional boundary. Physics of Fluids 6(7), 2253-2269 (1994)

48. Jenkins, J.T., Boundary conditions for collisional grain flows at bumpy, frictional walls. In Granular Gases, 125-139, Springer, Berlin (2001).